Geometry Optimization of Molecular Structures in Solution by the Polarizable Continuum Model

VINCENZO BARONE,[1] MAURIZIO COSSI,[1] JACOPO TOMASI[2]

[1]*Dipartimento di Chimica Università Federico II, I-80134 Napoli, Italy*
[2]*Dipartimento di Chimica e Chimica Industriale, Università di Pisa, 56124 Pisa, Italy*

Received 3 July 1997; accepted 28 September 1997

ABSTRACT: A new implementation of analytical gradients for the polarizable continuum model is presented, which allows Hartree-Fock and density functional calculations taking into account both electrostatic and nonelectrostatic contributions to energies and gradients for closed and open shell systems. Simplified procedures neglecting the derivatives of the cavity surface and/or using single spheres for XH_n groups have also been implemented and tested. The solvent-induced geometry relaxation has been studied for a number of representative systems in order to test the efficiency of the procedure and to investigate the role of different contributions. © 1998 John Wiley & Sons, Inc. J Comput Chem 19: 404–417, 1998

Keywords: geometry optimization; polarizable continuum model; density functionals; fixed cavity; mobile cavity

Introduction

The theoretical simulation of chemical processes in solution is difficult because of the large number of solvent molecules involved and the need for averaging over a huge number of configurations. This hinders a pure quantum mechanical approach to study the solvated systems and makes the use of simplified models necessary. Among them, approaches employing a polarizable continuum description of the solvent[1–3] appear particularly attractive when attention is focused on the effect of the medium on the quantum mechanical behavior of the solute. Furthermore, a reduced number of solvent molecules, whose behavior can strongly (and specifically) alter a chemical process, can be explicitly added to the solute, leading to a sort of supermolecule immersed in the polarizable continuum.[4]

In recent years, the reliability of these models has reached a remarkable level thanks to a number of developments. The most important are, in our

Correspondence to: V. Barone
Contract/grant sponsor: Italian Research Council (CNR)

CCC 0192-8651 / 98 / 040404-14

opinion, the use of cavities of realistic shape and an essentially exact solution of the electrostatic problem taking into account the solute polarization within the framework of refined quantum mechanical approaches. Together with semiempirical approaches,[5–7] which will not be considered further, we can mention implementations at the following levels: Hartree-Fock (HF),[8–10] density functional (DF),[9–16] many-body perturbation theory (MBPT),[17–19] generalized valence bond (GVB),[20] multiconfigurational self-consistent field (MCSCF),[21,22] and variational configuration interaction or coupled clusters with single and double replacements (CISD and CCSD, respectively).[19] Furthermore, the calculations have been made more efficient and user friendly thanks to specific software developments introduced in very effective quantum mechanical packages. Of course, alternative procedures (e.g., QM/MM,[23–25] polarizable dipoles[26,27]) provide interesting results and have been implemented in a number of packages, but they are outside the scope of the present study.

The next logical step is the computation of analytic energy derivatives in the presence of the solvent. As a matter of fact, geometry optimization is a prerequisite for any structural and dynamic analysis, and gradient-free procedures are highly inefficient for this purpose. Furthermore, determination of reaction paths and of thermodynamic parameters requires at least analytical gradients, if not Hessians.

Several implementations of analytic gradients in continuum solvent models have been reported recently.[8,9,13,28,29] However, most of them do not take into proper account all the terms contributing to the solvation energy (electrostatic, cavitation, and dispersion-repulsion). Furthermore, some simplifying assumptions are often made concerning the description of the solute electronic distribution (represented by one-center multipolar developments or by atomic charges) or the derivative of the cavity surface (neglected). Although a complete version of energy gradients in the framework of the so-called polarizable continuum model (PCM)[1,30,31] has been implemented in the HONDO package,[32] it allows only closed shell HF computations, without any provision for direct procedures, which are mandatory for the study of large systems. More recently, an effective version of the PCM has been implemented[33] in the Gaussian 94 (G94) package[34]; besides the computation of molecular energies and properties in solution, reported elsewhere,[35–37] this implementation has been extended to the analytical calculation of energy gradients that can be effectively employed in the various methods offered by G94 for geometry optimizations, locations of first-order saddle points, and in general the study of potential energy hypersurfaces.

An important feature of the present implementation is the capability of treating on the same footing all the contributions to the solvation energy derivatives for closed and open shell systems with, at least, the quantum methods routinely applicable for large molecules, namely, HF an DFT. In this paper we discuss some general aspects of our implementation of the PCM with special reference to the energy first derivatives; next, selected test cases are discussed in some detail, to show the range of applicability of the method and to give some warnings connected to its most effective use.

General Characteristics of PCM

PCM[30,31] belongs to the class of continuum polarizable solvation models:[1] The solute molecule, possibly supplemented by some specific solvent molecules, is placed in a cavity surrounded by an infinite polarizable dielectric. The molecular Hamiltonian is modified by the presence of the solvent

$$H_{solution} = H_{vacuum} + V_{solute-solvent}. \qquad (1)$$

H_{vacuum} is the Hamiltonian of the isolate solute (including the nuclear repulsion terms); the operator V linearly depends on the solute wave function and is expressed in terms of apparent polarization charges distributed on the cavity surface. The PCM procedure has also been extended to nonhomogeneous[38] and anisotropic dielectrics,[39,40] in which cases one has to consider polarization charges in the bulk of the solvent, too.

Apart from the contributions of vibrational, rotational, and translational motions of the solute nuclei, the molecular free energy in solution can be partitioned into four terms:

$$G^{sol} = G^{el} + G^{cav} + G^{disp} + G^{rep}. \qquad (2)$$

G^{el} collects the electrostatic contributions to the free energy, depending on the Hamiltonian (1):

$$G^{el} = \langle \Psi | H_{vacuum} + \tfrac{1}{2} V_{solute-solvent} | \Psi \rangle \qquad (3)$$

where Ψ is the normalized wave function of the solute.

The other terms in equation (2) affect only the solute energy and not its wave function[1]: They refer to the energy needed to form a suitable cavity in the solvent (free energy of cavitation, G^{cav}), to the dispersion solute-solvent free energy (G^{disp}), and to the part of the exchange solute–solvent interactions not included in the cavitation energy (G^{rep}). As is customary in the PCM method, G^{cav} is calculated by an adaptation to nonspherical solutes of the expression derived by Pierotti from the hard sphere theory,[41] whereas G^{disp} and G^{rep} are calculated following Floris and Tomasi's procedure,[42] with the parameters proposed by Caillet and Claverie.[43]

In the same way, the derivative of the molecular free energy in solution can be written

$$G^x = G^x_{es} + G^x_{cav} + G^x_{disp} + G^x_{rep} \tag{4}$$

where the superscript x indicates the partial derivative with respect to the parameter x. The detailed expressions for the nonelectrostatic terms have been given elsewhere,[32,44] so they are not discussed further.

The cavity where the solute is embedded is formed by the envelope of spheres centered on solute atoms or atomic groups; the cavity is then subdivided into small domains (called *tesserae*), where the polarization charges are placed. In standard PCM calculations the tesserae are drawn by projecting on each sphere the 60 triangular faces of an inscribed pentakisdodecahedron: the tesserae completely buried inside the cavity are discarded, and those cut by other spheres are replaced by suitable curved polygons. This procedure leaves hundreds to a few thousand tesserae for small to medium-sized solutes (say, up to 50 heavy atoms).

Molecular Free Energy in Solution

The boundary element method (BEM) version of the PCM procedure has been presented by Cammi and Tomasi[31] by defining a modified Fock operator obtained from the usual one- and two-electron operators for the isolated molecule. In a more general way, one can introduce unrestricted Hartree-Fock (UHF) or Kohn-Sham (UKS) formalisms using different generalized Fock matrices (F^α, F^β) for different spins.[45–47] In a finite basis (χ_μ, χ_ν ...) description, the $\mu\nu$ elements of these matrices are:

$$F^\alpha_{\mu\nu} = h_{\mu\nu} + J_{\mu\nu} + K^\alpha_{\mu\nu} + C^\alpha_{\mu\nu}(\uparrow\uparrow) + C^\beta_{\mu\nu}(\uparrow\downarrow) \tag{5a}$$

$$F^\beta_{\mu\nu} = h_{\mu\nu} + J_{\mu\nu} + K^\beta_{\mu\nu} + C^\beta_{\mu\nu}(\downarrow\downarrow) + C^\alpha_{\mu\nu}(\uparrow\downarrow) \tag{5b}$$

where h is the one-electron operator matrix and J the Coulomb operator matrix with elements

$$J_{\mu\nu} = \sum_{\lambda\sigma} P_{\lambda\sigma}(\mu\nu|\lambda\sigma) \tag{6}$$

and P is the one-particle density matrix. K^α and K^β are the exchange matrices for α and β electrons, respectively, defined as

$$K^\alpha_{\mu\nu} = \sum_{\lambda\sigma} P^\alpha_{\lambda\sigma}(\mu\lambda|\nu\sigma) \tag{7a}$$

$$K^\beta_{\mu\nu} = \sum_{\lambda\sigma} P^\beta_{\lambda\sigma}(\mu\lambda|\nu\sigma) \tag{7b}$$

in the HF approach, and as the functional derivatives of the corresponding exchange energies in DFT.[45–47] Finally, $C(\uparrow\uparrow)$ and $C(\uparrow\downarrow)$ are the functional derivatives of correlation functionals for electrons with parallel and antiparallel spins, respectively.[48] In the presence of the solvent, the $\mu\nu$ elements of the one-electron and Coulomb-operator matrices become

$$h'_{\mu\nu} = h_{\mu\nu} + \frac{1}{2}(j_{\mu\nu} + y_{\mu\nu}) \tag{8}$$

$$J'_{\mu\nu} = J_{\mu\nu} + X_{\mu\nu}. \tag{9}$$

To make the formulation clearer, the polarization charges are split into two parts, corresponding to the apparent charges created by the solute nuclei and by the solute electrons, respectively. Then, the matrices j, y, and X, respectively, express the interactions between the solute electrons and the polarization charges due to the solute nuclei, between the solute nuclei and the polarization charges due to the electrons, and between the electrons and the polarization charges due to electrons. Their elements are defined as[31]

$$j_{\mu\nu} = \sum_i^{tesserae} V^e_{\mu\nu}(i) q^N(i) \tag{10}$$

$$y_{\mu\nu} = \sum_i^{tesserae} V^N(i) q^e_{\mu\nu}(i) \tag{11}$$

$$X_{\mu\nu} = \sum_{i}^{tesserae} V^{e}_{\mu\nu}(i) q^{e}(i) = \sum_{i}^{tesserae} V^{e}_{\mu\nu}(i) \sum_{\lambda\sigma} P_{\lambda\sigma} q^{e}_{\lambda\sigma}(i) \quad (12)$$

where $V^N(i)$ is the potential exerted by the solute nuclei and $V^e_{\mu\nu}(i)$ is the potential due to the χ_μ, χ_ν basis functions on the i^{th} tessera. The polarization charges created by the nuclei and the electrons, respectively, can be collected in the vectors

$$q^N = -D^{-1}E^N \quad (13)$$

$$q^e_{\mu\nu} = -D^{-1}E^e_{\mu\nu}. \quad (14)$$

D is a geometrical matrix with elements

$$D_{ii} = \frac{1}{A_i}\left[\frac{4\pi\varepsilon}{\varepsilon - 1} - 2\pi(1 - \xi_i)\right] \quad (15)$$

$$D_{ij} = \frac{(r_i - r_j)}{|r_i - r_j|^3} \cdot n_i \quad (16)$$

where A_i is the area of the i^{th} tessera, r_i is the position vector of its representative point and n_i the corresponding unit vector normal to the surface (pointing outward). The vector E^N contains the normal component (i.e., the scalar product with n) of the electric field exerted by the solute nuclei on the tesserae; analogously, $E^e_{\mu\nu}$ contains the normal component of the field due to the χ_μ, χ_ν basis functions. The quantity

$$\xi_i = \left(\frac{A_i}{4\pi R_i^2}\right)^{1/2}, \quad (17)$$

where R_i is the radius of the sphere to which the i^{th} tessera belongs, is related to the curvature radius of the i^{th} tessera.[1]

The molecular wave function and the one-particle density matrix P can be determined finding the orbital coefficients with an SCF procedure identical to that followed in vacuo, using the generalized Fock operators defined in equation (5). In this framework, the electrostatic contribution to the SCF molecular free energy in solution is

$$G^{el}_{SCF} = E^{vac}_{SCF} + \frac{1}{2}trP(j + y) + \frac{1}{2}trPX + \frac{1}{2}U_{NN} \quad (18)$$

where

$$U_{NN} = \sum_{i}^{tesserae} V^N(i) q^N(i) \quad (19)$$

expresses the interaction between the solute nuclei and the polarization charges they create. E^{vac}_{SCF} is the molecular energy without the solvent contribution

$$E^{vac}_{SCF} = trPh + \frac{1}{2}trPJ + E_X + E_{corr} + V_{NN}, \quad (20)$$

formally identical to that defined for the isolated solute (notice, however, that one makes use of the density matrix P perturbed by the solvent). In eq. (20) V_{NN} is the solute nuclear repulsion energy, E_X is the exchange energy given by

$$E_x = -\frac{1}{2}tr[P^\alpha K^\alpha + P^\beta K^\beta] \quad (21)$$

in the HF theory, by the appropriate functional in DF approaches, and by an average of both in adiabatic connection models (ACMs)[47–49] such as the so-called B3LYP approach[50,51] that we will use in most computations. Finally E_{corr} is absent in the HF method and is given by appropriate functionals for parallel and antiparallel spins in DFT and ACM methods.[48]

Post-HF computations including the solvent contributions can be performed following two approaches.[18,37,52] In the first (referred to as *HFPC*), the post-HF energy and electron density are obtained using the polarization charges determined at the HF level. The second method (correlated polarization charges; CPC) requires a complete self-consistency between polarization charges and correlated density matrix, which can be reached by an iterative procedure, in which the polarization charges are computed with the post-HF matrix of the preceding cycle. Test calculations have shown that for the single reference approaches for which the density matrix can be obtained by the G94 package (MBPT, CISD, CCSD, and quadratic configuration interaction with single and double replacements; QCISD) the CPC convergence is usually reached in three cycles. As a consequence, a CPC calculation is about three times slower than the corresponding calculation in vacuo. On the other hand, the HFPC time request is quite the same as the corresponding in vacuo calculation, because the CPU time spent in the HF/PCM part is usually negligible with respect to the post-HF computation.

Normalization of the Polarization Charges

Gauss's law ensures that the total polarization charges appearing on the cavity surface obey the following relation

$$Q^N_{Gauss} = -\frac{\varepsilon - 1}{\varepsilon} \sum_k^{nuclei} Z_K \tag{22}$$

$$Q^e_{Gauss} = \frac{\varepsilon - 1}{\varepsilon} N^e \tag{23}$$

where Z^k is the k^{th} atomic number and N^e the total number of solute electrons. In computational practice, however, the actual values of the total polarization charges differ from those predicted by equations (22) and (23). This is due mainly to two factors: first, the numerical errors introduced by the discretization of the polarization charges on the surface and, second, the presence of a fraction of the solute electronic clouds outside the cavity.[30, 53, 54] The former error affects both q^N and q^e, whereas the latter affects q^e only. It has long been recognized[1, 29, 30] that this discrepancy could lead to nonnegligible errors in the calculated energies and electronic properties and that it is advisable to ''normalize'' the polarization charges, to get the correct theoretical values. Different normalization methods are available in the PCM version implemented in G94.[1, 54] In the most refined procedure, the polarization charges that should appear in the bulk of the dielectric owing to the escaped electronic tails are substituted by additional charges on the cavity surface, distributed according to the solute electronic density in each point of the surface.[54] This is the default method for single point computations but cannot be employed for analytical derivatives. Therefore, during geometry optimizations, a simpler normalization is activated in which each polarization charge is multiplied by a constant factor:

$$[q^N(i)]^{norm.} = f^N q^N(i) = \frac{Q^N_{Gauss}}{\sum_{tesserae} q^N(i)} q^N(i) \tag{24}$$

$$[q^e(i)]^{norm.} = f^e q^e(i) = \frac{Q^e_{Gauss}}{\sum_{tesserae} q^e(i)} q^e(i). \tag{25}$$

This choice is particularly effective for the calculations of derivatives with respect to nuclear coordinates, because large numbers of test calculations have shown that in this case the normalization factors f^N and f^e can be considered constant. Furthermore, solvation free energies evaluated with both normalization procedures are very similar, except for localized anions, and the situation should be even more favorable for energy derivatives. Thus the expressions derived in the next section refer to the derivatives of unnormalized polarization charges; the normalized values are obtained by multiplying by f^N and f^e.

Derivatives of the Electrostatic Free Energy in Solution

From equations (18) and (19), the derivatives of the electrostatic free energy in solution with respect to a parameter, x (nuclear coordinate, external field, and so on), can be written

$$(G^{el}_{SCF})^x = (E^{vac}_{SCF})^x + \frac{1}{2} trP(j^x + y^x) + \frac{1}{2} trPX^x + U^x_{NN} \tag{26}$$

where the expression E^{vac}_{SCF} is formally the energy derivative in vacuo using the density matrix and the Fock matrix perturbed by the solvent.[30]

Recalling equations (10–12), the derivatives appearing in equation (26) depend on the following terms.

$$[V^N(i)]^x; [q^N(i)]^x; \left[V^e_{\mu\nu}(i)\right]^x; \left[q^e_{\mu\nu}(i)\right]^x$$

The explicit form of these quantities, specialized for the case of the derivatives with respect to nuclear coordinates, is presented in the following; other formulations with respect to the dielectric constant and to external fields can be found elsewhere.[30, 55, 56] The nuclear and electronic potentials on tessera i are, respectively,

$$V^N(i) = \sum_k^{nuclei} \frac{Z_k}{|r_i - r_k|} \tag{27}$$

$$V^e_{\mu\nu}(i) = -\left\langle \chi_\mu \left| \frac{1}{|r_i - r|} \right| \chi_\nu \right\rangle. \tag{28}$$

The corresponding electric fields projected on the normal vector passing through the tessera i are

thus

$$E^N(i) = \sum_k^{nuclei} \frac{Z_k}{|r_i - r_k|^3}(r_i - r_k)\cdot n_i \quad (29)$$

$$E^e_{\mu\nu}(i) = \left\langle \chi_\mu \left| \nabla \frac{1}{|r_i - r|} \right| \chi_\nu \right\rangle \cdot n_i. \quad (30)$$

If x is a nuclear coordinate, we have

$$[V^N(i)]^x = -\sum_k^{nuclei} \frac{Z_k}{|r_i - r_k|^3}(r_i - r_k) \cdot \left[(r_i)^x - (r_k)^x\right] \quad (31)$$

$$\left[V^e_{\mu\nu}(i)\right]^x = -\left\langle (\chi_\mu)^x \left| \frac{1}{|r_i - r|} \right| \chi_\nu \right\rangle - \left\langle \chi_\mu \left| \frac{1}{|r_i - r|} \right| (\chi_\nu)^x \right\rangle - \left\langle \chi_\mu \left| \nabla \frac{1}{|r_i - r|} \right| \chi_\nu \right\rangle \cdot (r_i)^x \quad (32)$$

$$(q^N)^x = -(D^{-1})^x E^N - D^{-1}(E^N)^x \quad (33)$$

$$(q^e_{\mu\nu})^x = -(D^{-1})^x E^e_{\mu\nu} - D^{-1}(E^e_{\mu\nu})^x \quad (34)$$

Because

$$(D^{-1})^x = -D^{-1}D^xD^{-1}, \quad (35)$$

we can write

$$(q^N)^x = -D^{-1}[-D^xD^{-1}E^N + (E^N)^x] \quad (36)$$

$$(q^e_{\mu\nu})^x = -D^{-1}\left[-D^xD^{-1}E^e_{\mu\nu} + (E^e_{\mu\nu})^x\right]; \quad (37)$$

that is, recalling equations (13) and (14),

$$(q^N)^x = -D^{-1}\left[D^xq^N + (E^N)^x\right] \quad (38)$$

$$(q^e_{\mu\nu})^x = -D^{-1}\left[D^xq^e_{\mu\nu} + (E^e_{\mu\nu})^x\right]. \quad (39)$$

Using the shorthand notation

$$\frac{\partial}{\partial x}\left(\frac{p}{|p|^3}\right) = \frac{(p^x)}{|p|^3} - 3\frac{p\cdot p^x}{|p|^5}p \quad (40)$$

valid for any vector p, we have

$$(D_{ii})^x = -\frac{D_{ii}(A_i)^x}{A_i^2} + \frac{\pi}{\xi_l}\left[\frac{(A_i)^x}{4\pi R_i^2 A_i} - \frac{2}{4\pi R_i^3}(R_i)^x\right] \quad (41)$$

$$(D_{ij})^x = \frac{\partial}{\partial x}\left(\frac{r_i - r_k}{|r_i - r_k|^3}\right)\cdot n_i + \frac{r_i - r_k}{|r_i - r_k|^3}\cdot(n_i)^x \quad (42)$$

and

$$[E^N(i)]^x = \sum_k^{nuclei} Z_k\left[\frac{\partial}{\partial x}\left(\frac{r_i - r_k}{|r_i - r_k|^3}\right)\cdot n_i + \frac{r_i - r_k}{|r_i - r_k|^3}\cdot(n_i)^x\right] \quad (43)$$

$$\begin{aligned}\left[E^e_{\mu\nu}(i)\right] &= \frac{\partial}{\partial x}\left[\left\langle \chi_\mu \left| \nabla \frac{1}{|r_i - r|} \right| \chi_\nu \right\rangle \cdot n_i\right] \\ &= \left[\left\langle (\chi_\mu)^x \left| \nabla \frac{1}{|r - r_i|} \right| \chi_\nu \right\rangle + \left\langle \chi_\mu \left| \nabla \frac{1}{|r - r_i|} \right| (\chi_\nu)^x \right\rangle\right]\cdot n_i \\ &\quad - \left\langle \chi_\mu \left| \frac{\partial}{\partial x}\left(\frac{r_i - r}{|r_i - r|^3}\right) \right| \chi_\nu \right\rangle \cdot n_i \\ &\quad + \left\langle \chi_\mu \left| \nabla \frac{1}{|r_i - r|} \right| \chi_\nu \right\rangle \cdot (n_i)^x. \end{aligned} \quad (44)$$

The expressions listed above depend on integrals of the basis function derivatives, which are routinely computed by many computer programs, on simple derivatives of the nuclear positions and on the derivatives of the geometrical elements that define the surface tesserae (areas, sphere radii, tesserae position vectors, and unit vectors normal to the surface). The explicit expressions for these latter derivatives, namely, $(A_i)^x$, $(R_i)^x$, $(n_i)^x$ and $(r_i)^x$, are given by Cossi et al.[44] To the best of our knowledge, the PCM procedure is the only one that allows the analytical calculation of the derivatives of the geometrical elements of the surface tesserae. Other continuum solvation models that adopt cavities of molecular shape usually neglect these terms[9, 15] or use an approximate formulation.[29] Actually, also in the PCM procedure, it is possible to calculate the free energy derivatives neglecting the contribution of the tesserae geometrical elements: The corresponding expressions can be obtained from those listed above, by assuming that the geometrical derivatives vanish. This corresponds to calculate the energy derivatives assuming that the cavity is kept fixed and that it does not follow the infinitesimal motion of the solute atoms. This approximation, referred to as *fixed cavity* derivative calculation, can be useful in some cases,

when the analytical evaluation of such geometrical derivatives can raise problems related to numerical instabilities. Although the ''fixed cavity'' approximation appears reasonably good, as is shown below, it is certainly preferable to adopt the complete ''moving cavity'' procedure, which takes into account all the contributions to the energy derivatives, and also because the computer times are very similar for both approaches. Furthermore, the derivatives of the nonelectrostatic contributions to the free energy in solution depend only on the geometry of the cavity; therefore, ''fixed cavity'' derivatives of these terms are meaningless.

Shape of the Molecular Cavity

To obtain chemically accurate results, the cavity occupied by the solute must be described in a realistic way, mimicking the actual molecular shape. The PCM method adopts the GEPOL (generating polyhedra) procedure,[43,57–59] which builds the cavity as the envelope of spheres centered on individual atoms or atomic groups of the solute. Extensions to different kinds of tessellations[60] or procedures more suitable for very large solutes[61] are also available.

The various terms in equation (2) are calculated with slightly different definitions of the solute cavity. The cavitation energy is computed using a van der Waals surface (S_{vdW}), which is formed by the envelope of van der Waals spheres. Dispersion and repulsion contributions are calculated with a so-called solvent accessible surface (S_{SA}), i.e., a vdW surface with radii augmented by the solvent radius: S_{SA} corresponds to the surface described by the center of a probe sphere (with radius equal to the ''molecular radius'' of the solvent) rolling on S_{vdW}. For the electrostatic term, the procedure is as follows: First, the van der Waals radii are scaled by a factor $f > 1$ and then the resulting S_{vdW} is smoothed by adding some further spheres not centered on atoms. In this way, PCM approximates the so-called solvent excluding surface, S_{SE}, i.e., the contact surface of the solvent probe sphere rolling on S_{vdw}.

We have found, that, among the several available sets of radii for building these cavities, the van der Waals radii proposed by Pauling provide a sensible choice.[62,63] However, because a number of significant general trends are quite poorly reproduced by any set of standard radii, we are developing a new definition of molecular cavities referred to as *UATM* (united atom topological model). This model is based on chemical considerations (basically hybridization, formal charge, and first neighbor inductive effect), which, in turn, can be automatically derived from the geometry of the molecule.[5] As a matter of fact, at least for energy minima, a well-defined connectivity of atoms can be derived using interatomic distances only. Then, the number of first neighbors is sufficient to determine the hybridization and formal charge of each atom together with inductive effects. The aim of the UATM model is to extend computational approaches such as the G2 model[64] to condensed phases retaining the same chemical accuracy. As a consequence, we have developed the UAHF (united atom for Hartree-Fock) parametrization[65] to be used at the HF/6-31G* level, i.e., at the same level used by the G2 model to compute geometries and vibrational frequencies. Because the corresponding documentation is not yet available in the literature, we briefly resume the most significant points.

First, hydrogen atoms do not get individual spheres; they are included in the same sphere of the heavy atom they are bonded to. Second, the radius of all heavy atoms depends on the row of the periodic table to which they belong (1.50, 1.98, 2.08, and 2.38 Å for second, third, fourth, and fifth row, respectively), on their hybridization state, on their formal charge, on the number of bonded hydrogens (n_H), and on the number of bonded ''active'' atoms (*active* means having the same atomic number and the same hybridization state):

$$R(X) = R_{row} + \gamma_{row}\left(n_H + \frac{1}{2}n_{act} + \delta sp^2 + 1.5\delta sp\right) + \gamma_q q.$$

The value of γ_{row} is 0.09 for second-row atoms except for carbon (for which it is 0.18) and 0.13 for all other atoms; δsp^2 is 1 if X is in the sp^2 hybridization state and 0 otherwise, and analogously for δsp, whereas the hybridization correction for aromatic carbon atoms is taken as the average between sp^2 and sp values. Furthermore, the radius of aromatic carbons is reduced by 0.5 $\gamma(C)$ whenever they are bonded to at least one heteroatom or substituted carbon atom. The correction γ_q is introduced for the formal charge carried by atoms in ions and zwitterions (e.g., $|q| = 1$ for the O atom in CH_3O^- or in $CH_3OH_2^+$, and $|q| = 1/2$ for the O atoms in CH_3COO^-), the formal charge being determined on the basis of the number of bonds and the total molecular charge).

For all atoms bearing negative charges $\gamma_q = 0.3$, except for nitrogen, whose factor is $\gamma_q = 0.2$, whereas for atoms with a positive formal charge the factors are -0.26 (O^+), and -0.45 (P^+). No correction is necessary for N^+.

A further correction based on the number and nature of substituents is applied to sp^3 carbon atoms:

$$R(Csp^3) = R(C) - 0.09[\,n(Csp^2) + n(\mathrm{O}) + n(\mathrm{N}^+) + n(CX) + 1.5n(\mathrm{P}^+) + 2n(\mathrm{N}) + 3n(\mathrm{O}^-) - n(F)]$$

where CX indicates a substituted sp^3 carbon. Although the present parametrization would lead to discontinuities for situations involving changes of hybridization and/or formal charge for any atom, it is sufficient for the refinement of relative energy minima and for conformational studies. Extension to chemical reactions is in progress along the lines emphasized by Barone et al.[65]

Implementation Details

The present implementation fully exploits the highly efficient G94 routines for the computation of one-electron integrals in the calculation of the electrostatic potential and electric field on the surface tesserae; as a consequence, the parts of the PCM code devoted to the calculation of the polarization charges have been completely rewritten. The same is true for the derivatives of the electrostatic free energy: The reformulation of the code allows a substantial improvement of the original computer times.

The generalized Fock matrix is corrected for the effect of polarization charges at each SCF step, so that the solute wave function and the solvent polarization converge together. In every case the convergence thresholds on the SCF energy and density matrix are the same as in the corresponding calculations in vacuo.

Because finding the proper atomic and group radii for the UAHF cavities case by case can be quite tedious, a number of routines have been written and implemented in G94 that recognize the molecular topology and automatically assign the radii. Moreover, the recently developed PolyGen procedure[60] has been included in the present implementation; it allows the choice between a large variety of surface tessellations, and it has been used to test the dependence of calculated energies and gradients on the number of surface tesserae. In the following, the standard tessellation has been always used, because we found that increasing the number of tesserae does not change the results appreciably.

A last comment is in order about the CPU times required by PCM energy and gradient calculations, compared to the corresponding timings for isolated molecules. We have already reported that a complete computation of energy (i.e., always starting from the standard INDO guess of G94) is about 50% longer in solution than in vacuo for small solutes, and only $\sim 20\%$ longer in the case of larger systems. Taking into account that the PCM model has been implemented in such a way that it allows the contemporary calculation of energies in vacuo and in solution, a whole computation of solvation free energy is always less than 1.5 times longer than the computation in vacuo, and the ratio improves, increasing the dimension of the molecular systems (see Cossi et al.[33] and Barone et al.[65]). The situation is not very different concerning gradients, whose evaluation is at present between two and three times slower in solution than in vacuo. In practical terms this means that all the systems that can be studied in vacuo can be studied in solution too, because direct SCF techniques are applied in both cases.

Geometry Optimizations in Solution

The PCM energy gradients calculated by the procedures described above have been used to optimize the geometry of some molecules in solution with the so-called Berny algorithm[66] available in Gaussian94. The calculations have been performed at the HF and B3LYP levels using the 6-31G(d)[67] and the 6-311G(d,p)[68] basis sets. Diffuse functions on nonhydrogen atoms have been added when dealing with zwitterionic or anionic species, leading to 6-31 + G(d) and 6-311 + G(d,p) basis sets,[68] respectively. The solvent is always water at 25°C, with dielectric constant $\varepsilon = 78.4$. The role of different terms in the optimization of molecular structures in solution is illustrated in Table I for a number of small molecules and ions.

It is quite apparent that the energy derivatives of nonelectrostatic terms (cavitation and dispersion-repulsion) are one order of magnitude smaller than those of the electrostatic term. Also, the differences between the electrostatic derivatives evaluated employing mobile vs. rigid cavities are not

TABLE I.

Electrostatic and Nonelectrostatic Contributions to Solvation Free Energy and Its Gradient Obtained by Different Models for Typical Solutes.

Solute	QM method	Radii	ΔG_{es} (kcal/mol)	G_{cav} (kcal/mol)	G_{dis} (kcal/mol)	G_{rep} (kcal/mol)	Largest ΔG^x_{es} (a.u.)	Largest G^x_{cav} (a.u.)	Largest G^x_{dis} (a.u.)	Largest G^x_{rep} (a.u.)
H_2O	HF/6-31G(d)	Pauling	−9.1	4.9	−5.2	1.2	0.01518	0.00096	0.00030	0.00008
H_3O^+	HF/6-31G(d)	Pauling	−95.2	5.7	−5.9	1.2	0.09976	0.00091	0.00039	0.00007
OH^-	HF/6-31 + G(d)	Pauling	−96.3	4.3	−4.2	1.0	0.04471	0.00095	0.00027	0.00008
CH_3OH	HF/6-31G(d)	UAHF	−5.8	6.9	−8.3	1.9	0.02175	0.00107	0.00087	0.00017
CH_3O^-	HF/6-31 + G(d)	UAHF	−88.0	5.6	−9.1	3.3	0.09096	0.00094	0.00113	0.00175
CH_3CONH_2	HF/6-31G(d)	UAHF	−11.5	10.2	−11.9	2.6	0.02284	0.00111	0.00104	0.00158
CH_3COOH	B3LYP/6-31G(d,p)	UAHF	−13.3	10.0	−10.8	2.1	0.03306	0.00113	0.00087	0.00084
NH_3CHCOO^-	B3LYP/6-31 + G(d)	Pauling	−40.0	13.0	−12.4	2.2	0.05156	0.00108	0.00031	0.00019

very great. In spite of this general trend, the results in Table II show that optimized geometries obtained by different approximate methods differ somewhat from those obtained by the complete procedure, and this effect would be, of course, larger in less polar solvents.

Because computation times are comparable for all the approaches described above, we strongly suggest always employing the complete procedure. Fixed cavities can be profitably employed in the first steps of geometry optimizations; this procedure is generally less prone to numerical instabilities. On the other hand, neglecting nonelectrostatic terms does not yield an advantage. In any case, a much more effective procedure is to reduce the number of individual spheres, as is done in the UAHF model. As shown in Table II, geometries optimized by Pauling radii or by the UAHF model are very close, and the latter approach is faster and much more stable. Using these approaches, we were always able to converge geometry optimizations with the same Gaussian thresholds as for in vacuo computations ($4.5 \cdot 10^{-4}$ and $3.0 \cdot 10^{-4}$ a.u. for the maximum and average residual force, respectively, and $1.8 \cdot 10^{-3}$ and $1.2 \cdot 10^{-3}$ a.u. for the maximum and average predicted displacement, respectively).

Let us now discuss some chemically more interesting systems. As a first example we consider tautomeric equilibria in formamide and 2-pyridone either ruled by direct intramolecular proton transfer (PT) or assisted by an intervening water molecule (Fig. 1). The modifications of the geometrical parameters of formamide induced by the solvent are close to those shown in Table II for acetamide, whereas only very small modifications are obtained for formamidic acid. In particular, the main solvent effect is the lengthening of the C=O and the shortening of the C—N bond, clearly resulting from an increased weight of resonance structures involving charge separation.

The corresponding variations in 2-pyridone and 2-hydroxipyridine are shown in Figure 2. The role of the solvent reaction field in stabilizing the dipo-

TABLE II.

Principal Geometrical Parameters (Bond Lengths in Å, Valence Angles in Degrees) Optimized by Different Models for CH_3CONH_2 and CH_3COOH (syn) at the B3LYP/6-31G(d,p) Level.

	CH_3CONH_2						CH_3COOH syn		
Parameter	In vacuo	Pauling	UAHF	UAHF (only electr.)	UAHF (fixcav.)	Parameter	In vacuo	Pauling	UAHF
CO	1.215	1.233	1.230	1.231	1.231	C=O	1.203	1.212	1.211
CC	1.522	1.515	1.517	1.519	1.521	C—O	1.357	1.346	1.345
CN	1.369	1.350	1.351	1.353	1.356	CC	1.506	1.501	1.503
OCC	123.02	122.28	122.55	122.53	121.98	CC=O	126.13	125.81	125.63
NCC	114.70	115.26	115.02	115.14	115.42	CC—O	111.39	111.99	111.85

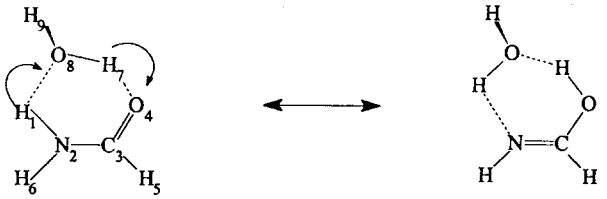

FIGURE 1. Assisted mechanism for the tautomerization of formamide.

lar resonance structure of 2-pyridone is again quite apparent from the lengthening of the CO bond (+0.016 Å) and from the concurrent shortening of the CN bond (−0.14 Å). To the contrary, the geometry of the enol tautomer is not affected by the presence of the solvent.

Thermodynamic and kinetic parameters of direct and water assisted tautomerization of formamide are summarized in Table III. In the gas phase, the B3LYP model predicts that formamide is more stable than formamidic acid by 12.6 kcal/mol and that PT is governed by a very high activation energy (46.2 kcal/mol). The specific interaction with a water molecule stabilizes the enol form by 2.5 kcal/mol and, especially, reduces the barrier governing PT to less than half the original value. All these results are in good agreement with previous post-HF computations.[4]

Solvent effects are significant for both direct and assisted mechanisms, increasing the endothermicity and the activation energy by 2–4 kcal/mol. Although geometry reoptimization in solution does not modify this general trend, it cannot be avoided in quantitative work, insofar as it further modifies thermodynamic and kinetic parameters by about 25% (see Table III). Very similar results are obtained for the thermochemistry of direct PT in 2-pyridone also reported in Table III.

Even greater effects are found concerning the presence of different conformers in vacuo and in solution. This point is illustrated by the results obtained for acetic acid at the B3LYP/6-31G(d,p) level (see Fig. 3). The energy difference between the two conformers in vacuo is 6.1 kcal/mol, compared to a value of 5.9 kcal/mol obtained at the MP3/6-311 + G(d,p) level[69] and to values of 5.1 and 4.8 kcal/mol obtained by standard density functionals in the local and gradient corrected formulation, respectively.[13] Thus, the B3LYP approach confirms its reliability in the field of noncovalent interactions. The energy difference between the two conformers is reduced to 2.9 kcal/mol in water solution, with a reduction (3.2 kcal/mol) very close to that obtained by standard density functionals employing the so-called COSMO continuum solvent model (3.3 and 3.1 kcal/mol using local and gradient corrected functionals, respectively).[13]

As a further example we have considered the simplest dipeptide analogue, namely, α-(formylamino)ethanamide (hereafter, AGP,i.e., analogue of glycine in a peptide) which has for a long

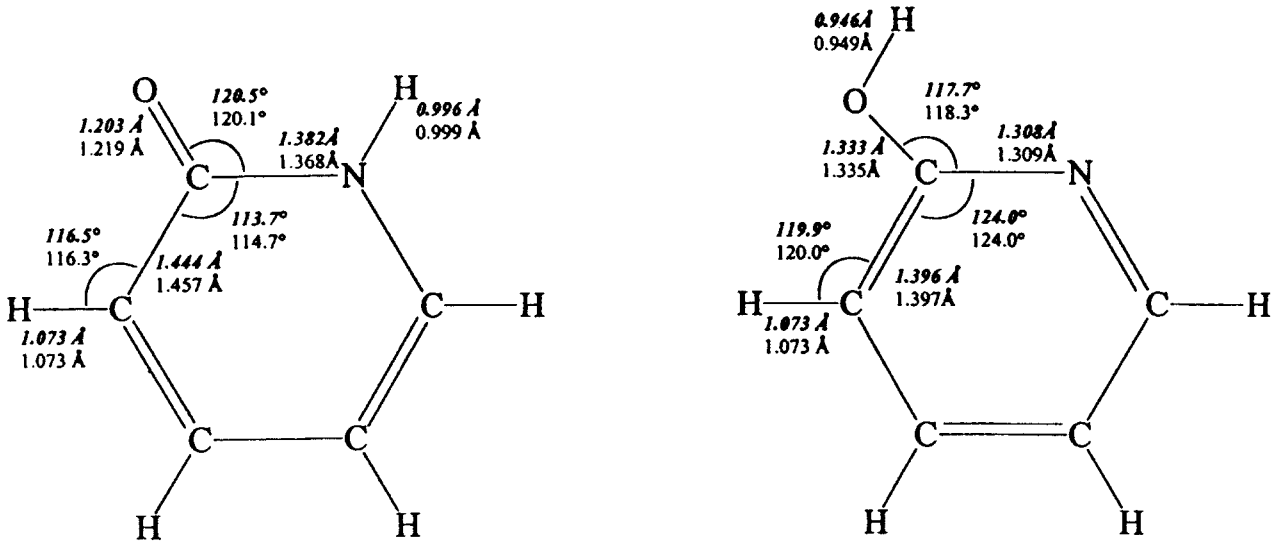

FIGURE 2. Principal geometrical parameters (bond lengths in Å and valence angles in degrees) optimized at the B3LYP / 6-31G(d) level for 2-pyridone and 2-hydroxipyridine both in vacuo (bold) and in aqueous solution (normal).

TABLE III.
Main Energy Contributions (kcal / mol) to the Endothermicities (ΔE) and Activation Energies ($\Delta E^{\#}$) for the keto / enol Tautomerizations of Formamide and of 2-Pyridone Computed at the B3LYP / 6-31G(d) Level.[a]

	In vacuo	Δ solvent direct	Δ geom. reopt. in solv.
Formamide			
ΔE_{dir}	12.6	3.3	0.3
$\Delta E^{\#}_{dir}$	46.2	4.0	0.4
ΔE_{ass}	10.1	2.3	0.6
$\Delta E^{\#}_{ass}$	19.4	1.4	0.6
2-Pyridone			
ΔE_{dir}	−1.6	−2.3	−0.5

[a]See text for the definition of direct and assisted mechanisms.

time served as one of the primary models for theoretical studies of backbone conformational equilibria in peptides and proteins (Fig. 4).[35,70] B3LYP/6-31G(d) computations indicate that four relative minima are present for the isolated molecule, with an energy spreading of less than 10 kcal/mol, the lowest ones corresponding to hydrogen bonded structures, namely, C_5 ($\phi = 180°$, $\psi = 180°$) and C_7 ($\phi = 80°$, $\psi = -60°$). The other minima correspond to distorted helices known as β_2 ($\phi = 120°$, $\psi = -20°$) and α' ($\phi = 180°$, $\psi = -60°$), respectively. These results are in agreement with previous HF computations[71] and with some experimental evidence of the occurrence of C_5 and C_7 conformers in low-polarity media and in argon matrix.[72]

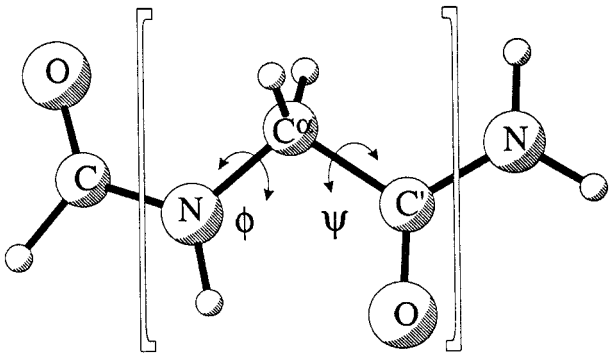

FIGURE 4. Atom labeling and structure of the C_5 energy minimum ($\phi = 180°$, $\psi = 180°$) for AGP.

An increase in solvent polarity leads to the destabilization of hydrogen-bonded structures (C_7) in favor of helical ones, which in highly polar solvents, such as water, eventually become the absolute energy minima.[73] B3LYP/6-31G(d) computations coupled to the PCM continuum model for the solvent confirm this trend and show that the differences in stability are attenuated by solvation. As a matter of fact, the energy difference between the most and least stable conformations is reduced from 8 kcal/mol in the gas phase to less than 3 kcal/mol in water solution (see Fig. 5).

It is noteworthy that the computed electrostatic contributions to solvation energies generally follow the computed dipole moments, except in the case of the β_2 conformer, whose stabilization is particularly high. Geometry reoptimization in water leads to the same lengthening of C=O bonds and shortening of C—N bonds observed for acetamide, owing to the usual stabilization of ionic

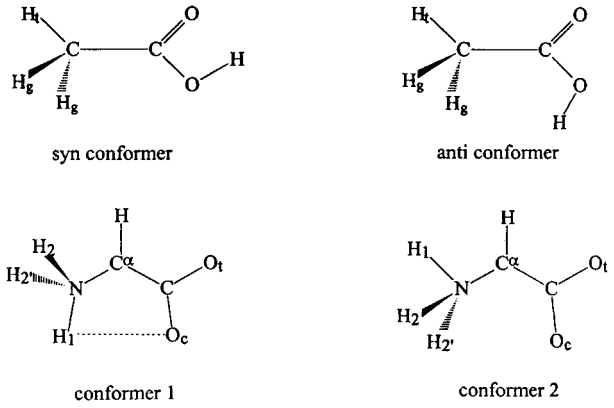

FIGURE 3. Structures and atom numbering for the conformers of acetic acid and of the zwitterionic form of glycine radical.

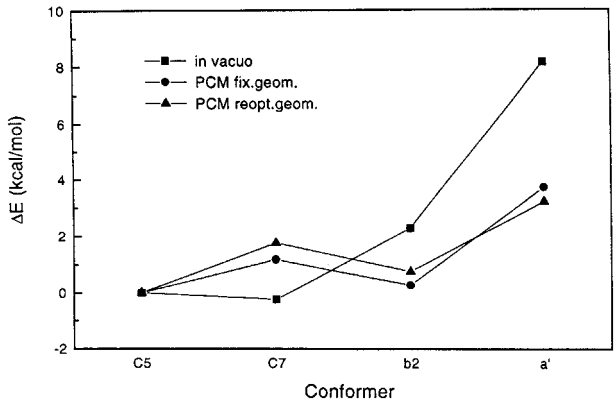

FIGURE 5. Relative stabilities of different conformers of AGP obtained at the B3LYP / 6-31G(d) level in vacuo and in aqueous solution.

resonance forms by polar solvents. However, for AGP also, the ψ dihedral angle is significantly modified in C_7 (from 60° to 69°) and β_2 (from −20° to 15°) structures. The energetic effect of these modifications is not very strong, but it further destabilizes the C_7 conformer with respect to other energy minima (see Fig. 5).

To test our procedure on open shell systems, we optimized the geometry of the zwitterionic form of the glycine radical[74] (Fig. 3) both in vacuo and in water solution. The structure having an internal hydrogen bond (conformer 1) is not an energy minimum in vacuo and leads to the neutral form, whereas the other structure (conformer 2) is a stationary point (see Table IV). The situation is very different in solution, where the conformer 1 is the most stable structure for the zwitterionic form, though remaining less stable than the neutral radical.[75]

The solvent induces noticeable geometry rearrangements in this system, in particular concerning the planarity of the radical center; it is noteworthy that this geometrical change has a negligible effect on the solvation energy but significantly affects the values of electronic properties such as the isotropic hyperfine couplings (hfc).

TABLE IV.

Geometrical Parameters (Bond Lengths in Å, Valence Angles in Degrees) and Isotropic hfc (in G) for the Zwitterionic Form of Glycine Radical.[a]

	conformer1 in vacuo[a]	conformer1 in water	conformer2 in water
NC	1.486	1.458	1.451
CC	1.500	1.481	1.482
CO_c	1.271	1.268	1.272
CO_t	1.245	1.264	1.262
CH	1.084	1.082	1.081
NH_1	1.023	1.026	1.037
NH_2	1.031	1.029	1.029
NCC	110.87	118.13	115.91
CCO_c	111.44	116.11	115.11
CCO_t	115.78	115.80	116.76
CCH	132.11	126.26	126.58
CNH_1	115.19	111.62	106.03
CNH_2	107.31	111.81	112.83
H_2NCC	54.42	59.00	119.68
aC^{α}	48.82 (47.08)	44.75	44.60
aO_4	0.17 (−0.91)	−1.30	−1.85
aH^{α}	−24.12 (−24.66)	−24.46	−23.98
aO_5	−4.00 (−2.58)	−2.84	−2.41
aC′	−9.69 (−9.93)	−10.65	−10.80
aN	−2.38 (−2.30)	−2.54	−2.47
aH_7	0.35 (0.19)	0.44	0.55
aH_8	24.96 (23.85)	26.27	26.09

[a]All the computations have been performed at the B3LYP/6-31 + G(d,p) level.
[b]Values in parenthesis are from water using the geometry optimized in vacuo.

Although the equations for analytical second derivatives of the PCM model were developed some time ago,[31] they have not yet been implemented. We considered it interesting, however, to analyze solvent-induced vibrational shifts on a typical compound using finite differences of analytical gradients. To this end we have selected the formamide molecule[76] studied at the B3LYP/6-31G(d) quantum mechanical model, which is able to give accurate vibrational frequencies in vacuo.[77,78] The results are shown in Table V.

The geometrical rearrangements induced by the solvent are reflected well in the harmonic frequencies. Although no mode mixing is observed in going from the gas phase to aqueous solution, a large shift of the carbonyl stretching is computed ($+90$ cm^{-1}). Other significant solvent shifts are calculated for the CH stretching ($+63$ cm^{-1}) and, especially, for the out-of-plane bending of the amine moiety ($+200$ cm^{-1}). The solvent effect on the CO stretching is in agreement with experimental observations on several carbonyl compounds,[79] and all the computed shifts are consistent with the stabilization by the solvent of the resonance form involving a formal charge separation.

Conclusions

We have reported the essential details of an effective implementation of analytical gradients of the PCM model in the framework of the Gaussian package. From a technical point of view, this implementation allows both a complete procedure including electrostatic and nonelectrostatic terms and some simplified approaches neglecting, for instance, cavity derivatives. A number of examples have shown that the procedure is reliable and stable, allowing, especially when coupled to the effective UAHF model, one to optimize also flexible structures with the same thresholds as those of in vacuo optimizations. Computation times are already reasonable and can be further improved. Thanks to the availability of direct procedures for energies and gradients and to the reasonable number of finite elements allowed by the effective GEPOL approach, quite large systems are already amenable to complete studies in solution. The situ-

TABLE V.
Harmonic Wave Numbers (cm^{-1}) and (in Parenthesis) IR Intensities (in km / mol) Calculated In Vacuo and In Water for Formamide at the B3LYP / 6-31G(d) Level Using Pauling Radii.

Vib. mode	In vacuo	In water	Exp.[a]
NH_2 inversion	162.1 (249)	365.6 (345)	303 vs
NCO bend	562.8 (12)	581.2 (26)	564 m
NH_2 twist	649.6 (21)	681.8 (16)	682 m
CH out pla.	1,047.2 (0)	1,070.5 (1)	1,047 w
NH_2 wagging	1,054.4 (3)	1,070.7 (5)	1,185 w
CN stretch	1,275.5 (95)	1,301.6 (111)	1,261 s
CH in plane bend	1,432.5 (54)	1,405.1 (30)	1,400 m
NH_2 bend	1,620.8 (68)	1,588.1 (119)	1,579 s
CO stretch	1,836.0 (352)	1,746.2 (651)	1,740 us
CH stretch	2,949.2 (110)	3,012.0 (89)	2,884 m
NH_2 symm. str.	3,596.6 (314)	3,574.8 (123)	3,427 m
NH_2 asymm. str.	3,741.2 (37)	3,713.8 (130)	3,548 m

[a]Reference 67.

ation will be even more favorable thanks to further technical improvements only briefly outlined in this paper. From a more chemical point of view, the present approach has allowed us to obtain interesting results about intramolecular proton transfer, relative stabilities of different conformers, and stabilization of zwitterionic forms also for open shell species.

In summary, we think that the most significant outcome of this study and related studies is that a quantitative description of physicochemical processes in solution is becoming more and more feasible owing to the development of integrated tools consisting of effective electronic methods coupled to refined polarizable continuum models for the description of environmental effects. Promising results are being obtained also for chemical reactions, and the whole computational protocol is or will shortly be available to other researchers in the field through standard quantum chemical packages.

References

1. J. Tomasi and M. Persico, *Chem. Rev.* **94**, 2027 (1994).
2. J. L. Rivail, D. Rinaldi, and M. F. Ruiz-Lopez, Liquid state quantum chemistry, in: *Computational Chemistry: Review of Current Trends*, J. Lesczynski, ed. World Scientific, Singapore, 195.
3. C. J. Cramer, and D. J. Truhlar, in: *Reviews in Computational Chemistry*, K. B. Lipkowitz and B. Boyd, eds., VCH Publishers, New York, 1995, Vol. 6, p. 1.
4. V. Barone, and C. Adamo, *J. Phys. Chem.*, **99**, 15062 (1995).
5. C. C. Chambers, G. D. Hawkins, C. J. Cramer, and D. G. Truhlar, *J. Phys. Chem.*, **100**, 16385 (1996).
6. M. M. Karelson, A. R. Katrizky, M. Szafran, and M. C. Zerner, *J. Org. Chem.*, **54**, 6030 (1989).
7. P. A. Basch, M. J. Field, and M. Karplus, *J. Am. Chem. Soc.*, **109**, 8092 (1987).
8. I. Tuñón, M. F. Ruiz-Lopez, D. Rinaldi, and J. Bertrán, *J. Comput. Chem.*, **17**, 148 (1996).
9. T. N. Truong, and E. V. Stefanovich, *J. Chem. Phys.*, **103**, 3709 (1995).
10. J. B. Foresman, T. A. Keith, K. B. Wiberg, J. Snoonian, and M. J. Frisch, *J. Phys. Chem.*, **100**, 16098 (1996).
11. A. Fortunelli, and J. Tomasi, *Chem. Phys. Lett.*, **231**, 34 (1994).
12. R. J. Hall, M. M. Davison, N. A. Burton, and I. H. Hiller, *J. Phys. Chem.*, **99**, 921 (1995).
13. J. Andzelm, C. Kölmel, and A. Klamt, *J. Chem. Phys.*, **103**, 9312 (1995).
14. G. J. Tawa, R. L. Martin, L. R. Pratt, and T. V. Russo, *J. Phys. Chem.*, **100**, 1515 (1996).
15. J. L. Chen, L. Noodleman, D. A. Case, and D. Bashford, *J. Phys. Chem.*, **98**, 11059 (1994); W. H. Richarson, C. Peng, D. Bashford, L. Noodleman, and D. A. Case, *Int. J. Quantum Chem.*, **61**, 207 (1997).
16. M. F. Ruiz-López, F. Bohr, M. T. C. Martins-Costa, and D. Rinaldi, *Chem. Phys. Lett.*, **221**, 109 (1994).
17. J. L. Rivail, *C. R. Acad. Sci. II*, **311**, 307 (1980).
18. F. J. Olivares del Valle and J. Tomasi, *Chem. Phys.*, **150**, 139 (1991).
19. A. Fortunelli, *Theochem.*, **357**, 117 (1995).
20. D. J. Tannor, B. Marten, R. Murphy, R. A. Friesner, D. Sitkoff, A. Nicholls, M. Ringnala, W. A. Goddard III, and B. Honig, *J. Am. Chem. Soc.*, **116**, 11875 (1994).
21. K. V. Mikkelsen, H. Ågren, H. J. A. Jensen, and T. Helgaker, *J. Chem. Phys.*, **89**, 3086 (1988); K. V. Mikkelsen, A. Cesar, H. Ågren, and H. J. A. Jensen, *J. Chem. Phys.*, **103**, 9010 (1995).
22. M. Reguero, R. R. Pappalardo, M. A. Robb, and H. S. Rzepa, *J. Chem. Soc. Perkin Trans.* **2**, 1499 (1993); R. R. Pappalardo, M. Reguero, M. A. Robb, and M. J. Frisch, *Chem. Phys. Lett.*, **212**, 12 (1993).

23. A.Warshel and M. Levitt, *J. Mol. Biol.*, **103**, 227 (1976).
24. M. J. Field, P. Basch, and M. Karplus, *J. Comput. Chem.*, **11**, 700 (1990); A. Warshel, in: *Computer Modeling of Chemical Reactions in Enzymes and in Solutions*, John Wiley & Sons, New York, 1991; J. Gao, in: *Reviews in Computational Chemistry*, K. B. Lipkowitz, D. B. Boyd, eds., VCH, New York (1995).
25. M. J. Harrison, N. A. Burton, I. H. Hiller, and I. R. Gouldd, *Chem. Commun.*, 2769 (1996); M. Perakila and P. A. Kollman, *J. Am. Chem. Soc.*, **119**, 1189 (1997); V. Moliner, A. J. Turner, and I. Williams, *Chem. Commun.*, 1271 (1997).
26. J. Florian and A. Warshel, *J. Phys. Chem.*, **101**, 5583 (1997).
27. N. O. J. Malcolm and J. J. W. McDouall, *J. Mol. Struct. (Theochem.)*, **366**, 1 (1996).
28. C. M. Cortis, J. M. Langlois, M. D. Beachy, and R. A. Friesner, *J. Chem. Phys.*, **105**, 5472 (1996).
29. V. Dillet, D. Rinaldi, J. Bertrán, and J. L. Rivail, *J. Chem. Phys.*, **104**, 9437 (1996).
30. S. Miertus, E. Scrocco, and J. Tomasi, *Chem. Phys.*, **55**, 117 (1981).
31. R. Cammi and J. Tomasi, *J. Chem. Phys.*, **100**, 7495 (1994).
32. M. Cossi, J. Tomasi, and R. Cammi, *Int. J. Quantum Chem. Quantum Chem. Symp.*, **29**, 695 (1995).
33. M. Cossi, V. Barone, R. Cammi, and J. Tomasi, *Chem. Phys. Lett.*, **255**, 327 (1996).
34. M. J. Frisch, G. W. Trucks, H. B. Schlegel, P. M. W. Gill, B. G. Johnson, M. A. Robb, J. R. Cheeseman, T. A. Keith, G. A. Petersson, J. A. Montgomery, K. Raghavachari, M. A. Al-Laham, V. G. Zakrewski, J. V. Ortiz, J. B. Foresman, J. Cioslowski, B. B. Stefanov, A. Nanayakkara, M. Challacombe, C. Y. Peng, P. Y. Ayala, W. Chen, M. W. Wong, J. L. Andres, E. S. Replogle, R. Gomperts, R. L. Martin, D. J. Fox, J. S. Binkley, D. J. DeFrees, J. Baker, J. P. Stewart, M. Head-Gordon, C. Gonzalez, and J. A. Pople, *Gaussian 94* (Revision D.4), Gaussian, Inc., Pittsburgh, 1996.
35. C. Adamo, V. Dillet, and V. Barone, *Chem. Phys. Lett.*, **263**, 113 (1996).
36. V. Barone, *Chem. Phys. Lett.*, **262**, 201 (1996).
37. N. Rega, M. Cossi, and V. Barone, *J. Chem. Phys.*, **105**, 11060 (1996).
38. M. Cossi, B. Mennucci, and J. Tomasi, *Chem. Phys. Lett.*, **228**, 165 (1994).
39. B. Mennucci, M. Cossi, and J. Tomasi, *J. Chem. Phys.*, **102**, 6837 (1995).
40. B. Mennucci, M. Cossi, and J. Tomasi, *J. Phys. Chem.*, **100**, 1807 (1996).
41. R. A. Pierotti, *Chem. Rev.*, **76**, 717 (1976).
42. F. M. Floris and J. Tomasi, *J. Comput. Chem.*, **10**, 616 (1989); F. M. Floris, J. Tomasi, and J. L. Pascual-Ahuir, *J. Comput. Chem.*, **12**, 784 (1991).
43. J. L. Pascual-Ahuir, E. Silla, J. Tomasi, and R. Bonaccorsi, *J. Comput. Chem.*, **8**, 778 (1987).
44. M. Cossi, B. Mennucci, and R. Cammi, *J. Comput. Chem.*, **17**, 57 (1996).
45. J. A. Pople, P. M. W. Gill, and B. G. Johnson, *Chem. Phys. Lett.*, **199**, 557 (1992).
46. B. G. Johnson and M. J. Frisch, *J. Chem. Phys.*, **100**, 7429 (1994).
47. V. Barone, in: *Recent Advances of Density Functional Theory, Part I*, D. P. Chong, ed., World Scientific, Singapore, 1996, p. 287.
48. A. D. Becke, *J. Chem. Phys.*, **104**, 1040 (1996).
49. A. D. Becke, *J. Chem. Phys.*, **98**, 5648 (1993).
50. B. J. Stevens, F. J. Devlin, C. F. Chablowski, and M. J. Frisch, *J. Phys. Chem.*, **98**, 11623 (1994).
51. V. Barone, *Chem. Phys. Lett.*, **226**, 392 (1994).
52. J. G. Angyan, *Chem. Phys. Lett.*, **241**, 51 (1995).
53. A. Klamt and V. Jonas, *J. Chem. Phys.*, **105**, 9972 (1996).
54. B. Mennucci and J. Tomasi, *J. Chem. Phys.*, **106**, 5151 (1997).
55. R. Cammi, M. Cossi, and J. Tomasi, *J. Chem. Phys.*, **104**, 4611 (1996).
56. R. Cammi, M. Cossi, B. Mennucci, and J. Tomasi, *J. Chem. Phys.*, **105**, 10556 (1996).
57. J. L. Pascual-Ahuir and E. Silla, *J. Comput. Chem.*, **11**, 1047 (1991).
58. E. Silla, I. Tuñón, and J. L. Pascual-Ahuir, *J. Comput. Chem.*, **12**, 1077 (1991).
59. J. L. Pascual-Ahuir, E. Silla, and I. Tuñón, *J. Comput. Chem.*, **15**, 1127 (1994).
60. C. Pomelli, J. Tomasi, in preparation.
61. R. Cammi, M. Cossi, B. Mennucci, C. Pomelli, and J. Tomasi, *Int. J. Quantum Chem.*, **60**, 1165 (1996).
62. R. C. Weast, ed., *Handbook of Chemistry and Physics*, CRC Press, Cleveland (1981).
63. M. Bachs, F. J. Luque, and M. Orozco, *J. Comput. Chem.*, **15**, 446 (1994).
64. L. A. Curtiss, K. Raghavachari, and J. A. Pople, *J. Chem. Phys.*, **98**, 1293 (1993).
65. V. Barone, M. Cossi, and J. Tomasi, *J. Chem. Phys.*, **107**, 3210 (1997).
66. H. B. Schlegel, *J. Comput. Chem.*, **3**, 214 (1982).
67. P. C. Hariharan and J. A. Pople, *Theor. Chim. Acta*, **28**, 213 (1973).
68. R. Krishnan, J. S. Binkley, R. Seeger, and J. A. Pople, *J. Chem. Phys.*, **72**, 650 (1980); T. Clark, J. Chandrasekhar, G. W. Spitznagel, and P. R. Schleyer, *J. Comput. Chem.*, **4**, 294 (1983).
69. K. B. Wiberg and K. E. Laidig, *J. Am. Chem. Soc.*, **109**, 5935 (1987).
70. P. Amodeo and V. Barone, *J. Am. Chem. Soc.*, **114**, 9085 (1992).
71. I. R. Gould, W. D. Cornell, and I. H. Hillier, *J. Am. Chem. Soc.*, **116**, 9250 (1994).
72. T. Yamazaki and A. Abe, *Biopolymers*, **27**, 969 (1988).
73. V. Madison and K. D. Kopple, *J. Am. Chem. Soc.*, **102**, 4855 (1980).
74. V. Barone, C. Adamo, A. Grand, and R. Subra, *Chem. Phys. Lett.*, **242**, 351 (1995).
75. V. Barone, C. Adamo, A. Grand, F. Jolibois, Y. Brunel, and R. Subra, *J. Am. Chem. Soc.*, **117**, 12618 (1995).
76. M. Rasanen, *J. Mol. Struct.*, **101**, 275 (1983).
77. V. Barone, *J. Chem. Phys.*, **101**, 10666 (1994); *Theor. Chim. Acta*, **91**, 113 (1995).
78. G. Rauhut and P. Pulay, *J. Phys. Chem.*, **99**, 3093 (1995).
79. M. K. Wong, K. B. Wiberg, and M. J. Frisch, *J. Am. Chem. Soc.*, **114**, 1645 (1992).